Computer-Assisted Processing of Current Step Signals in Single Blocking Impact Electrochemistry

Arthur Langlard, Hassiba Smida, Romain Chevalet, Christine Thobie-Gautier, Mohammed Boujtita, Estelle Lebègue

Computer-Assisted Processing of Current Step Signals in Single Blocking Impact Electrochemistry

Arthur Langlard, Hassiba Smida, Romain Chevalet, Christine Thobie-Gautier, Mohammed Boujtita, and Estelle Lebègue*

Nantes Université, CNRS, CEISAM, UMR 6230, F-44000 Nantes, France

KEYWORDS: single blocking impacts, redox probe, liposomes, Gram-negative bacteria, current step signals, computer-assisted processing

ABSTRACT: Current step signals related to single entity collisions in blocking impact electrochemistry were analyzed by computer-assisted processing for estimating the size distribution of various particles. In this work, three different types of entities were studied by single blocking impact electrochemistry: polystyrene nanospheres (350 nm-diameter) and microspheres (1 µm-diameter), phospholipid liposomes (300 nm-diameter) and two different strains of Gram-negative bacillus bacteria (*Escherichia coli* and *Shewanella oneidensis*). The size estimations of these different entities from the current step signals analysis were compared and discussed according to the shape and size of each entity. From the magnitude of the current step transient, the size distribution of each entity was calculated thanks to a new computer program assisting in the detection and analysis of single impact events in chronoamperometry measurements. The data processing showed that the size distribution obtained from electrochemical data agreed with the dynamic light scattering and atomic force microscopy data for nanospheres and liposomes. In contrast, the size estimation calculated from electrochemical data was underestimated for microspheres and bacteria. We demonstrated that our computer program was efficient for detecting and analyzing the collision events in single blocking impact electrochemistry for various entities from spherical hard nanoparticles to micron-sized rod-shaped living bacteria.

INTRODUCTION

Electroanalytical chemistry greatly evolved with the continuous improvement of instrumentation sensitivity and especially with the development of the electrochemical detection of individual entities.[1–4] In this context, single-entity electrochemistry, namely discrete collisions technique or nano-impacts method based on stochastic events, is a useful tool for the detection via single impacts of various micro- and nano-entities such as nanoparticles, cells, bacteria, vesicles, viruses, proteins in solution at a polarized ultramicroelectrode (UME).[5–14] Single-entity electrochemistry method can provide unique information on various individual entities through the detection of discrete events in contrast to ensemble (bulk) measurements.[15–19] For each impact event, the chronoamperometry measurement (i–t curve) shows a specific signal corresponding to an "impact" of the entity onto the UME surface. Subsequent analysis of electrochemical impact events in the i–t curve can provide useful data, such as the concentration and the size of the colliding entities.[20–23]

A great advantage of single-entity electrochemistry is the possibility to detect and analyze various targets at the single-cell scale, especially insulating entities by using the blocking impact method.[2,10,13,22,24–26] Because of its easy-to-perform principle, versatility and efficiency, blocking impact electrochemistry was quickly extended to the detection of various micro- and nano-entities, with a specific interest in single collisions of bio-targets such as proteins, viruses, and bacteria.[7,13,21,24,27–29] Blocking impact electrochemistry deals with single collisions of insulating (bio)entities on the UME surface polarized at the redox potential of the electroactive probe in solution, involving in most cases a "current step" signal in the i–t curve, corresponding to an impact event. Usually, the UME is biased at a potential where the electron transfer reaction is at a diffusion-limited steady state in a solution containing the target entity and a redox species. As an entity adsorbs onto the UME, it locally hinders the diffusive flux of redox species to the electrode, causing a drop of faradaic current (step-shaped transient).[21,25,26] The current step magnitude in blocking impact experiments depends on the size of the adsorbed entity, the size and the shape of the UME, the type and the concentration of the redox probe, the applied potential and the location of the entity adsorbed onto the UME surface.[21,24–26,30–32] Several studies showed a significant enhancement of the entity sizing precision in single blocking impact electrochemistry by using a hemispherical UME rather than a disk UME or by applying lower overpotentials for mitigating edge effects.[25,30]

A simple estimate of the radius of the disk surface occupied by a single spherical entity adsorbed (r_{ads}) onto the UME disk surface can be calculated from the following equation.[13,33]

$$r_{ads} = r_e \sqrt{\frac{\Delta i_{ss}}{i_{ss}}} \qquad (1)$$

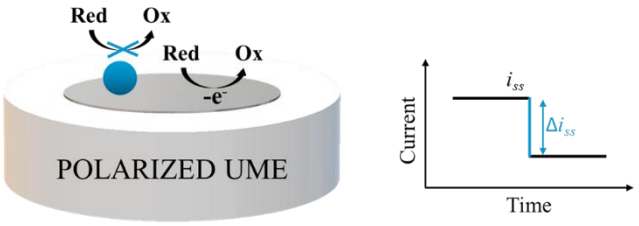

Figure 1. Schematic representation of a single impact of a spherical insulating particle on the polarized UME disk surface (left) and the resulting current step signal observed in the *i*–*t* curve (right).

In Eq. 1, r_e is the UME disk radius, Δi_{ss} is the current step magnitude, and i_{ss} is the steady-state current before the analyzed current step (Figure 1) [9]. Because Eq. 1 does not take into account the edge effect inherent in electrochemical blocking experiments on disk UMEs and the shape of the entity, estimating the size of non-spherical entities such as bacteria with this equation is questionable.[9,25,31,32] To the best of our knowledge, Eq. 1 was mainly used for the radius estimation of different entities in the work of Dick *et al.* dealing with single blocking impacts of antibodies, enzymes, DNA and polystyrene nanospheres[13] and also, for determining the volume of red blood cells.[34] The radius values estimated from the current steps' magnitudes and Eq. 1 for these different species had the same order of magnitude as those obtained from their crystallographic data.[13] Nevertheless, this size estimation method was not repeated and extended to various entities such as liposomes and bacteria.

We present herein a comparative study aiming to detect and analyze current step signals related to single collisions of three different entities usually studied in our lab (polystyrene spheres, liposomes and bacteria), based on blocking impact electrochemistry. We propose a computer program for detecting and analyzing each current step transient in the *i*–*t* curves recorded at the oxidation potential of the ferrocyanide redox probe (+0.8 V vs Ag/AgCl) on a 10 µm-diameter Pt disk UME in the presence of different entities (Figure 2): 350 nm-diameter and 1 µm-diameter polystyrene spheres (sizes provided by the supplier), 300 nm-diameter phospholipid liposomes (hydrodynamic diameter estimated by dynamic light scattering) and two different strains of Gram-negative bacillus bacteria (*Escherichia coli* and *Shewanella oneidensis*) with a length of about 2 µm and a width of about 0.5 µm.[9,26,27] The radius estimation of these three different targets using Eq. 1 is also discussed in this work. Indeed, our study aims to clearly show that Eq. 1 is only suitable for estimating the size of spherical entities whose diameter is sufficiently smaller than the disk UME diameter. The development of this computer program is interesting in the context of high throughput data processing like the electrochemical detection of impact events, where the study of single entities one by one is more advantageous than measuring numerous entities as a whole.[35] In addition, the availability of a computer program in open and free source is a great advantage for a systematic and an accurate data processing of various blocking impact experiments. In contrast, this study is not focused on the impact event frequency related to the entities concentration in solution because several previous reports already reviewed this point[9,27,33,36] and it is not the aim of this present work.

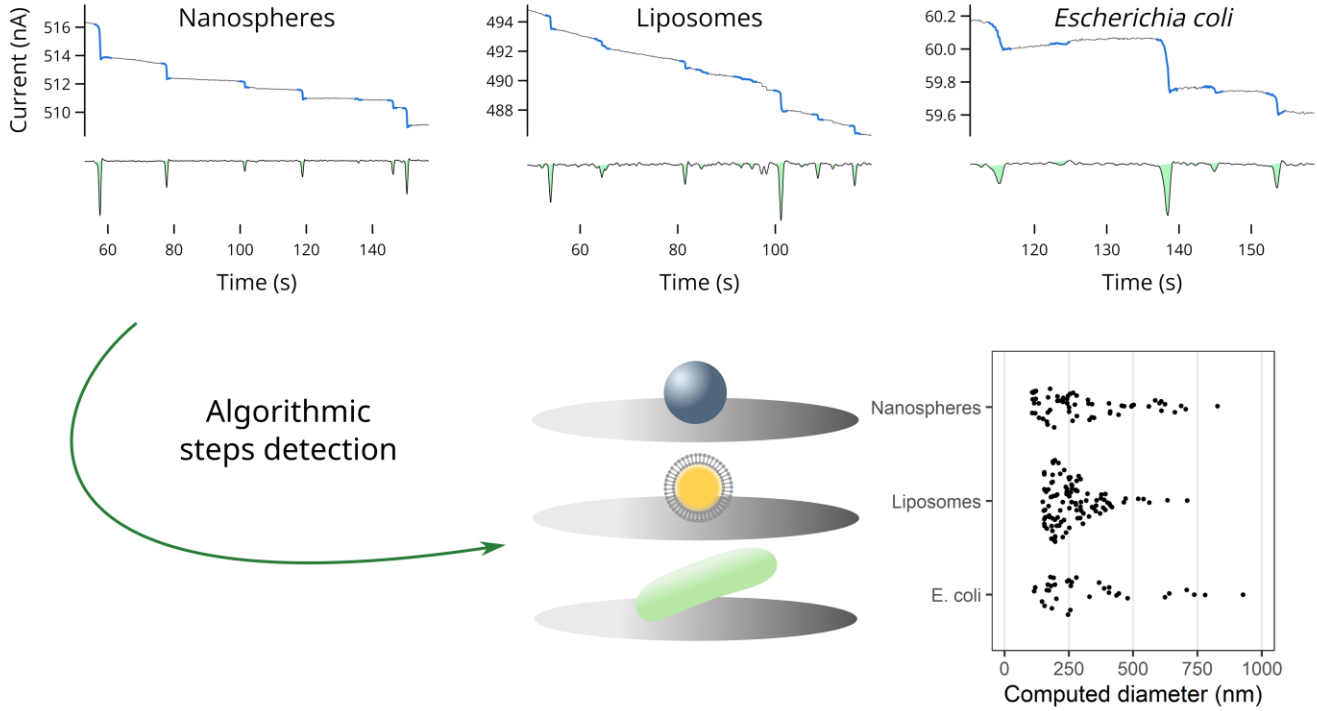

Figure 2. Computer-assisted processing of current step signals related to collisions of three different entities (polystyrene spheres, phospholipid liposomes and Gram-negative bacillus bacteria) in single blocking impact electrochemistry.

MATERIALS AND METHODS

Materials and Reagents

All chemicals were reagent grade and used as purchased without further purification. Water used in each experiment was deionized water. Chloroform (>99%) was purchased from Fisher Scientific. Potassium ferrocyanide trihydrate (98.5%) was purchased from Acros Organics. Phosphate buffer (PB) solution at 1.0 M and pH 7.4 (25 °C) was purchased from Sigma Aldrich and stored at 3 °C. Potassium and sodium chloride were purchased from Sigma Aldrich. Iron(III) nitrate nonahydrate was purchased from Acros Organics. Phosphate buffered saline (PBS) used for experiments with bacteria was composed of 0.1 M commercial phosphate buffer solution, 50 mM KCl and 50 mM NaCl (pH 7.4 at 25 °C) and was stored at 3 °C. 1,2-dimyristoyl-sn-glycero-3-phosphocholine (DMPC) lipids were purchased as a powder from Sigma Aldrich (Avanti Polar Lipids) and stored at -18 °C. Luria–Bertani (LB) medium, LB agar plates and glycerol were obtained from Sigma Aldrich. Polystyrene spheres were obtained from Polyscience Europe GmbH.

Liposomes preparation

As we previously reported,[8] liposomes suspensions were prepared by dissolving 10 mM DMPC lipid (powder) in chloroform (1 mL) for the complete dissolution of lipids. The homogeneous mixture was placed under a nitrogen (N_2) flow for 30 minutes for the complete evaporation of chloroform. The dry lipid film was hydrated by the addition of an aqueous solution (1 mL of 0.5 M $K_4Fe(CN)_6$ as a redox probe), then the mixture was sonicated for 1 minute and heated on a hot plate at 50 °C for 30 minutes under stirring. The DMPC liposome solutions were extruded using 400 nm diameter polycarbonate membranes from Avanti Polar Lipids. The extrusion of liposomes was carried out with the extruder set from Avanti Polar Lipids including a mini-extruder, 2 syringes of 1 mL, polycarbonate membranes of 0.4 µm and filter supports. The liposomes suspension was passed through the extruder 9 times, which was kept warm at 50 °C, to obtain DMPC liposomes suspensions. Then, size-exclusion chromatography (PD-10 Desalting Columns, Cytiva) was performed to remove the redox probe that was not encapsulated inside the liposomes. By using a 0.1 M PB aqueous solution at pH 7.4, the first fraction containing the liposomes was kept. The end is detected by the precipitation of a Prussian blue compound upon contact with an iron(III) nitrate aqueous solution, indicating the presence of ferrocyanide ions in the eluate. This final step for redox DMPC liposomes (encapsulating ferrocyanide ions) typically yields a nanomolar range DMPC liposomes suspension that is stored at 3 °C for 3 days. The size distribution of the liposomes was determined by dynamic light scattering (DLS) carried out on a Vasco Kin™ Particle Size Analyzer using the NanoKin® software. These redox liposomes encapsulating ferrocyanide ions are mainly used for electrolysis collisions where they are studied in our group for bacterial toxins detection[8], but in this study, their redox property was not a relevant parameter.

Electrochemical measurements

The electrochemical experiments were performed at room temperature (21 ± 2 °C) using a SP-300 potentiostat (Bio-Logic) with an ultra-low current module and with a three-electrode cell placed in a Faraday cage (BioLogic FC-45) and using the EC-Lab software. The 10 µm diameter Pt disk UME purchased from CH Instruments (CHI107) was used as the working electrode. Pt wire was used as a counter electrode and pseudo-reference electrode. For checking the stability of the Pt pseudo-reference, all the potentials were controlled and reported with an Ag/AgCl (3 M NaCl) reference electrode (Figure S1). The electrochemical aqueous solution was composed of 0.5 M $K_4Fe(CN)_6$ without PB or 50 mM $K_4Fe(CN)_6$ with 0.1 M PBS pH 7.4. For all chronamperometry *i-t* curves recorded, the sample interval (in sampling time) was 100 ms. Before each electrochemical experiment, the Pt UME was mechanically polished using wetted fine grit silicon carbide paper from Struers (4000-grit SiC) and washed in water.

Computer-assisted processing of electrochemical data

An algorithm was developed with Python to perform current steps detection and measurements from the raw *i-t* curves. First, the expected transient current caused by the growth of the diffusion layer was subtracted. The Shoup-Szabo equation for a disk-UME was fitted to the signal during the specific period 0.1 s – 20 s (not at the very beginning to avoid saturation caused by the charging of the double-layer capacitance and not too long to avoid taking into account too many current steps) by adjusting the electrode radius.[37] This results in a theoretically flat current between the steps. Then, a differentiation method was applied to convert downward steps into negative peaks: for every signal value, the average of the next five values (which correspond to a 0.5 s period with our 10 Hz sampling rate) was subtracted to the average of the previous five values, resulting in a transformed signal *T*. The resulting peaks were detected with the signal.find_peaks() function of Scipy, and the prominence value required for this function was evaluated for each sample. We chose to set this value to the magnitude of the signal's background fluctuations, which was estimated by a measurement of the standard deviation of the signal over a 5 s period (Table S1).

Integration of the peaks gives the step's magnitude. For each peak, the integration was not calculated down to zero but to a line connecting the two bases of the peak. These points were obtained by calculating the difference with neighboring values, starting from the middle of the peak, until they fell below a threshold of 10^{-14} A – indicating a stable signal. We found that the value of 10^{-14} was a satisfactory compromise for detecting the settling of the noisy signal. This gives the positions of the left and right feet of the peak, which were used as baseline's extremities for the integration. Figure S2 illustrates each of these algorithmic steps. Steps with a calculated magnitude below 3 times the standard deviation of the background signal were not considered significant and were ignored. Graphs and statistical plots were done using the Veusz software[38] and RStudio.[39] A copy of the Python script is available in the following repository: https://gitlab.univ-nantes.fr/E17E952C/steps-detection

RESULTS AND DISCUSSION

All blocking impact experiments presented in this study were performed by recording a chronoamperometry measurement at the steady-state current oxidation potential of ferrocyanide ions (+0.8 V vs Ag/AgCl) in an aqueous solution composed of 0.5 M $K_4Fe(CN)_6$ (for nanospheres and liposomes) or 50 mM $K_4Fe(CN)_6$ and 0.1 M PBS at pH 7.4 (for microspheres and bacteria) in the electrochemical cell. The different suspensions of entities were directly added into the electrochemical solution, either from the commercial sample for polystyrene spheres, or from those previously prepared with liposomes and bacteria (suspended in a phosphate buffer solution as described in the Experimental section). Before the blocking impact measurements, cyclic voltammetry and *i–t* curves were recorded in an entities-free solution in order to check the steady-state current of the working electrode (10 µm-diameter Pt UME) according to its size and the concentration of the redox probe.[19] Once these control experiments were performed, several *i–t* curves were recorded at room temperature in the presence of different target entities (between 10^9 and 10^{10} entities mL^{-1}) added in the electrochemical cell containing the aqueous redox solution. The three different types of entities studied by single blocking impact electrochemistry were polystyrene spheres, liposomes and bacteria: 350 nm-diameter nanospheres and 1 µm-diameter microspheres, 300 nm-diameter liposomes and two different strains of Gram-negative bacillus bacteria (*E. coli* and *S. oneidensis*). In this study, the linear relationship between collision frequency and entity concentration[13,28,36,40] were not investigated because we focused on the analysis of current step signals in the blocking impact experiments with various entities. Also, different 10 µm diameter Pt disk UMEs were used as working electrodes for recording all *i–t* curves presented in this study, consequently the baseline current differed slightly from one measurement to another.

Typical *i–t* curves recorded on 10 µm-diameter Pt UME in the presence of nanospheres (blue), liposomes (red), microspheres (blue), *E. coli* (green) and *S. oneidensis* (orange) are shown in Figure 3. As expected in these electrochemical blocking impact experiments, several current step signals were observed, corresponding to single entity impact events onto the Pt UME surface.[9,13,26,33,36] Generally, current transients have the shape of a step with stable edges (Figure 3 and Figure S3), indicating that most of the impacting entities hit and remain adsorbed onto the Pt UME surface after a collision. A significant difference in the stability of the background current over the entire duration of the measurement was observed for these different entities, especially for bacteria collisions (Figure S3). This phenomenon is inherent to living entity collisions, which involve a specific activity of biological species adsorbed onto the polarized UME. Such behavior is exemplified by the *S. oneidensis* bacteria, where the outer membrane redox proteins play a crucial role in the cell's mobility and adhesion onto a polarized surface, as demonstrated by our previous work.[29]

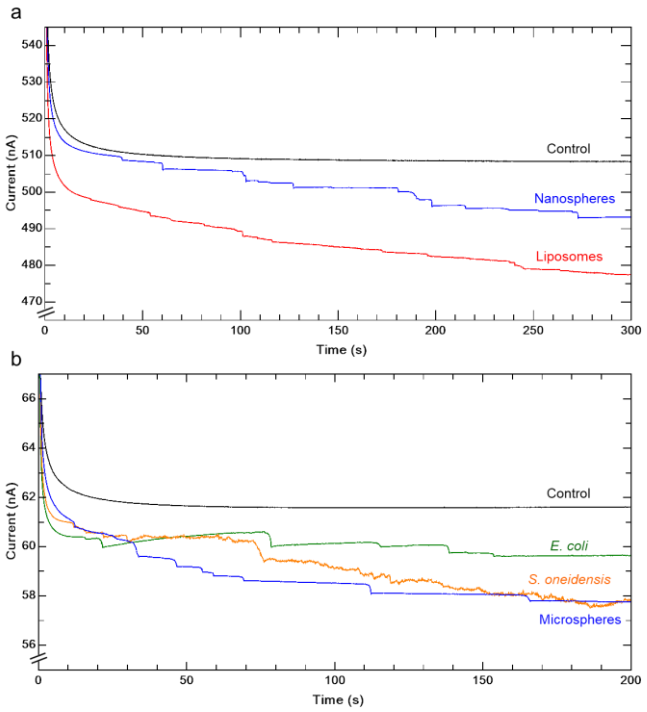

Figure 3. *i–t* curves recorded on a 10 µm-diameter Pt UME at +0.8 V vs Ag/AgCl in (a) 0.5 M $K_4Fe(CN)_6$ and (b) 50 mM $K_4Fe(CN)_6$ 0.1 M PBS at pH 7.4 at room temperature, in the absence (black) and in the presence of (a) ~10^9 liposomes mL^{-1} (red), ~10^{10} nanospheres mL^{-1} (blue) and (b) ~10^9 cells mL^{-1} of *E. coli* (green), *S. oneidensis* (orange), ~10^9 microspheres mL^{-1} (blue).

In order to have a representative sampling, the analysis of current step transients was carried out for three *i–t* curves recorded in the same experimental conditions for each target entity (Figure S3) and the collected data were reported in a spreadsheet file provided in Supporting Information (Appendix: Current steps analysis). The average diameter of an adsorbed entity with its standard deviation provided in the first row of Table 1 was calculated from Eq. 1 for each current step signal reported in the Appendix file. Note that, in this work, only current steps with a current drop at least three times higher than the noisy current fluctuations were considered as collision events.

The values reported in the first row of Table 1 for nanospheres (360 nm) and liposomes (310 nm) show a good correlation between the average diameter calculated from electrochemical data and the size distribution obtained from DLS data (Figure S4 and Figure S5) reported in the third row. These two entities are quite similar in size and shape because nanospheres are spherical hard nanoparticles (350 nm-diameter) while liposomes are spherical soft entities (300 nm-diameter). Also, the ratio between the projected area of the adsorbed entity and the disk UME is about 0.1% (as observed in AFM imaging reported in Figure S7), which seems an optimal value for reaching a good estimation of the entities's size from Eq. 1.

Table 1. Average diameter with its standard deviation of adsorbed entities estimated from Eq. 1 for the current step signals of the *i*–*t* curves recorded on a 10 µm-diameter Pt UME at +0.8 V vs Ag/AgCl reported in Figure S3 (d_{ads}) and from the output of the program (d_{prog}) compared to the average hydrodynamic diameter determined by DLS reported in Figures S3, S4 and S5 (d_{DLS}).

	Nanospheres	Liposomes	Microspheres	*E. coli*	*S. oneidensis*
d_{ads} (nm)	360 ± 180	310 ± 100	680 ± 230	570 ± 280	640 ± 160
d_{prog} (nm)	310 ± 190	270 ± 110	570 ± 450	420 ± 520	650 ± 270
d_{DLS} (nm)	400	300	1200	1600	1700

In contrast, the average diameter of spherical microspheres calculated from electrochemical data in the first row of Table 1 (680 nm) is underestimated in comparison to the values obtained from DLS data (1.2 µm) reported in the third row of Table 1 and the AFM measurements (Figure S8). This result can be explained by the ratio between the projected area of the adsorbed particle and the disk UME surface (1%), which is 10 times higher for microspheres than with nanospheres. Therefore, the larger size of these particles increases the likelihood of stacking incoming microspheres on top of already adsorbed ones onto the UME (as observed in AFM imaging, Figure S8). In this case, the current step magnitude measured for a single impact is lower than expected if the microsphere is stacked. Moreover, particles colliding onto the glass sheath, near the conductive surface of the electrode, would slightly restrict the diffusive flux, resulting in a lower current step. This signal would be interpreted either as a small particle, or be buried below the noise level and interpreted as experimental noise. In these conditions, the use of Eq. 1 for estimating the size of the colliding entity is only limited to giving an order of magnitude of the size with a significant underestimation. This observation is extended to the case of bacteria where the average diameter reported in the first row of Table 1 is about 570 nm and 640 nm for *E. coli* and *S. oneidensis*, respectively. The average hydrodynamic diameter determined by DLS (Figure S6) is about 1600 nm and 1700 nm for *E. coli* and *S. oneidensis*, respectively (the third row of Table 1). These rod-shaped bacteria have a length of about 2 µm and a width of about 0.5 µm,[9,26,27] therefore a single adsorbed bacterium occupies theoretically about 1 µm² onto the Pt UME surface (see AFM imaging in Figure S8). For these living and non-spherical entities, Eq. 1 seems quite unsuited for calculating an average diameter, especially because bacteria behave differently onto the polarized UME surface according to their specific properties and surface charge.[26,28,29] The broad size distribution obtained with single impact measurements for all entities is probably due to the edge effect inherent to the UME disk, as the current density at the edge is ten times higher than at the center of the electrode. This observation was previously reported in different studies dealing with single blocking impacts of polystyrene spheres and bacteria.[26,27,31,33]

Because of the time-consuming and repetitive aspects of manual data processing for each current step signal in *i*–*t* curves, we developed a data processing program for detecting and analyzing the collision events in single blocking impact experiments. To the best of our knowledge, most of the computer programs reported in the literature for single collision data processing deal with current spikes analysis corresponding to the electrolysis impact method.[41,42] The details of the method and algorithm used for our program were reported in the Materials and Methods section, and in the Supporting Information file. All *i*–*t* curves presented in Figure S3 were processed by our program and as an example, Figure 4 shows an extract of the computer-assisted data processing for liposomes and *E. coli*. The data processing performed with our program for nanospheres, microspheres and *S. oneidensis* is reported in Figure S9.

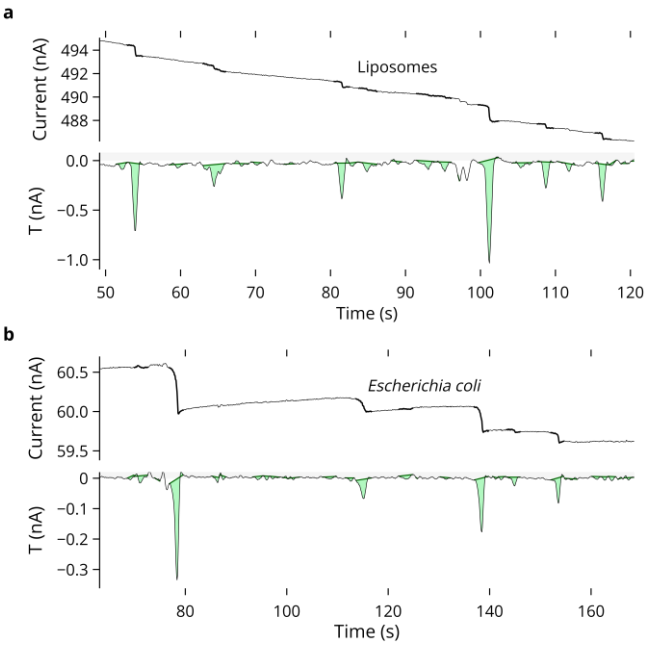

Figure 4. Computer-assisted processing of current step signals detected in *i*–*t* curves and related to single impacts onto the Pt UME surface of liposomes (a) and *E. coli* bacteria (b). Overlaid bold curves indicate the time span used for the integration of a detected step.

As presented in Figure 4, each current step signal corresponds to a peak in the differentiate curve *T*, facilitating the detection and visibility of single impact events in *i*–*t* curves. Also, with the computer-assisted processing, the number of current step signals detected in all *i*–*t* curves were significantly higher than with the manual processing

reported in the spreadsheet (Appendix: Current steps analysis). The calculation parameters of the program were chosen so that they could be adapted for all different target entities from spherical hard nanoparticles to micron-sized rod-shaped living bacteria in order to propose a relevant overall procedure.

Computer-assisted analysis of the current steps' magnitudes uses Eq. 1 to calculate the diameter of entities adsorbing onto the Pt UME. The diameter values of each entity are reported in Figure 5 and computed average sizes are indicated in the second row of Table 1. Compared with the average diameters reported in the first row of Table 1, the computed average sizes are overall lower and with a broader size distribution. This result can be explained by a higher number of current step signals detected in *i–t* curves with the computer-assisted processing, especially more current steps with a lower magnitude. This trend is particularly visible in Figure 5 where a wide size distribution is observed for the five entities studied. Only in the case of liposomes, a normal distribution can be observed on the computed average diameter, in contrast to the other entities, particularly microspheres, where the size distribution is significantly larger and dispersed (Figure 5). The diagram presented in Figure 5 shows that the use of Eq. 1 to estimate the entities' sizes is only suitable for nanometric and spherical particles but not for micrometric and non-spherical ones in our experimental conditions (10 µm diameter Pt disk UME), in agreement with our previous observations with the manual processing.

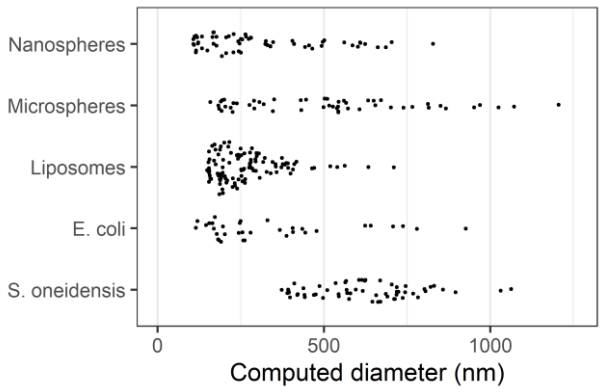

Figure 5. Distributions of diameter values of adsorbed entities estimated from Eq. 1 for the current step signals detected and analyzed by our computer program in *i–t* curves for liposomes, nanospheres, microspheres, *E. coli* and *S. oneidensis*.

As demonstrated, the computer-assisted processing for current steps analysis in *i-t* curves is an efficient and low-time-consuming strategy for blocking impact experiments with various entities. Regardless of the method used for detecting the steps, a large spread in steps magnitudes are converted to surprisingly broad size distributions. This highlights that, not only the size, but also the aspect and location of the entity on the UME surface during its impact are all parameters shaping the step of current. In contrast, the number of previous collisions and entities adsorbed seem to have little to no effect on the magnitude of the current step corresponding to a blocking impact event in our experimental conditions (Figure S10).

CONCLUSIONS

In this work, we focused on the detection and analysis of current step signals corresponding to single impact events onto the disk UME surface for estimating the size of various entities in blocking impact electrochemistry experiments. Ferrocyanide ions were used as a redox probe in an aqueous solution and a 10 µm-diameter Pt disk UME was used as a working electrode for all chronoamperometry measurements. The three different types of entities studied by single blocking impact electrochemistry were polystyrene nanospheres (350 nm-diameter) and microspheres (1 µm-diameter), phospholipid liposomes (300 nm-diameter) and two different strains of Gram-negative bacillus bacteria (*E. coli* and *S. oneidensis*). First, an estimation of the average diameter was performed from the current step transients' magnitudes by using the equation linking the radius of the disk UME to the radius of the disk surface occupied by the adsorbed entity. This size estimation proved to be relevant for nanospheres and liposomes but significantly less efficient for microspheres and bacteria with an underestimation of their size. This difference could be related to the ratio between the projected area of the adsorbed entity and the disk UME, and also the non-spherical shape of bacteria. We also developed an efficient computer program for assisting the detection and analysis of current step transients in *i–t* curves, avoiding the time-consuming and repetitive aspects of manual data processing. The size distribution obtained by this processing agreed with our previous results, showing a larger and more dispersed distribution for microspheres and bacteria than liposomes and nanospheres. Our computer program was efficient for detecting and analyzing the collision events in single blocking impact electrochemistry for various entities from spherical hard nanoparticles to micron-sized rod-shaped living bacteria. In the near future, it could be extended to other types of single impact electrochemistry such as catalysis and electrolysis events with a relevant overall procedure for these types of collisions.

ASSOCIATED CONTENT

The Supporting Information is available free of charge.
Cyclic voltammograms; standard deviations of the background current; computer processing steps; *i–t* curves; dynamic light scattering data; atomic force microscopy imaging; relation between diameter vs impact number.

AUTHOR INFORMATION

Corresponding Author

* Estelle Lebègue – Nantes Université, CNRS, CEISAM, UMR 6230, F-44000 Nantes, France; https://orcid.org/0000-0002-8610-0891; Email: estelle.lebegue@univ-nantes.fr

Author Contributions

Arthur Langlard: Data curation, Formal analysis, Investigation, Conceptualization, Methodology, Visualization, Writing – original draft, Writing – review & editing. Hassiba Smida: Data curation, Formal analysis, Investigation. Romain Chevalet:

Data curation, Formal analysis, Investigation. Christine Thobie-Gautier: Investigation, Writing – review & editing. Mohammed Boujtita: Investigation, Writing – review & editing. Estelle Lebègue: Conceptualization, Investigation, Funding acquisition, Supervision, Writing – original draft, Writing – review & editing.

Notes

The authors declare no competing financial interest.

ACKNOWLEDGMENT

The authors thank Dr. Catarina M. Paquete for providing the bacterial strains and François-Xavier Lefèvre for the training in AFM. This work was supported by the French National Research Agency (ANR-21-CE42-0007-01, ELIPOX) and the Pays de la Loire Regional Council (Rising stars program, e-NANOBIO).

REFERENCES

(1) Sundaresan, V.; Do, H.; Shrout, J. D.; Bohn, P. W. Electrochemical and Spectroelectrochemical Characterization of Bacteria and Bacterial Systems. *Analyst* **2021**, *147* (1), 22–34. https://doi.org/10.1039/D1AN01954F.

(2) Goines, S.; Dick, J. E. Review—Electrochemistry's Potential to Reach the Ultimate Sensitivity in Measurement Science. *J. Electrochem. Soc.* **2019**, *167* (3), 037505. https://doi.org/10.1149/2.0052003JES.

(3) Moussa, S.; Mauzeroll, J. Review—Microelectrodes: An Overview of Probe Development and Bioelectrochemistry Applications from 2013 to 2018. *J. Electrochem. Soc.* **2019**, *166* (6), G25–G38. https://doi.org/10.1149/2.0741906jes.

(4) Sekretareva, A. Single-Entity Electrochemistry of Collision in Sensing Applications. *Sens. Actuators Rep.* **2021**, *3*, 100037. https://doi.org/10.1016/j.snr.2021.100037.

(5) Sepunaru, L.; Tschulik, K.; Batchelor-McAuley, C.; Gavish, R.; Compton, R. G. Electrochemical Detection of Single E. Coli Bacteria Labeled with Silver Nanoparticles. *Biomater. Sci.* **2015**, *3* (6), 816–820. https://doi.org/10.1039/C5BM00114E.

(6) Dick, J. E. Electrochemical Detection of Single Cancer and Healthy Cell Collisions on a Microelectrode. *Chem. Commun.* **2016**, *52* (72), 10906–10909. https://doi.org/10.1039/C6CC04515D.

(7) Dick, J. E.; Hilterbrand, A. T.; Boika, A.; Upton, J. W.; Bard, A. J. Electrochemical Detection of a Single Cytomegalovirus at an Ultramicroelectrode and Its Antibody Anchoring. *Proc. Natl. Acad. Sci.* **2015**, *112* (17), 5303–5308. https://doi.org/10.1073/pnas.1504294112.

(8) Luy, J.; Ameline, D.; Thobie-Gautier, C.; Boujtita, M.; Lebègue, E. Detection of Bacterial Rhamnolipid Toxin by Redox Liposome Single Impact Electrochemistry. *Angew. Chem. Int. Ed.* **2022**, *61* (6), e202111416. https://doi.org/10.1002/anie.202111416.

(9) Smida, H.; Lefèvre, F.-X.; Thobie-Gautier, C.; Boujtita, M.; Paquete, C. M.; Lebègue, E. Single Electrochemical Impacts of Shewanella Oneidensis MR-1 Bacteria for Living Cells Adsorption onto a Polarized Ultramicroelectrode Surface. *ChemElectroChem* **2023**, *10* (1), e202200906. https://doi.org/10.1002/celc.202200906.

(10) Quinn, B. M.; van't Hof, P. G.; Lemay, S. G. Time-Resolved Electrochemical Detection of Discrete Adsorption Events. *J. Am. Chem. Soc.* **2004**, *126* (27), 8360–8361. https://doi.org/10.1021/ja0478577.

(11) Xiao, X.; Fan, F.-R. F.; Zhou, J.; Bard, A. J. Current Transients in Single Nanoparticle Collision Events. *J. Am. Chem. Soc.* **2008**, *130* (49), 16669–16677. https://doi.org/10.1021/ja8051393.

(12) Dunevall, J.; Fathali, H.; Najafinobar, N.; Lovric, J.; Wigström, J.; Cans, A.-S.; Ewing, A. G. Characterizing the Catecholamine Content of Single Mammalian Vesicles by Collision–Adsorption Events at an Electrode. *J. Am. Chem. Soc.* **2015**, *137* (13), 4344–4346. https://doi.org/10.1021/ja512972f.

(13) Dick, J. E.; Renault, C.; Bard, A. J. Observation of Single-Protein and DNA Macromolecule Collisions on Ultramicroelectrodes. *J. Am. Chem. Soc.* **2015**, *137* (26), 8376–8379. https://doi.org/10.1021/jacs.5b04545.

(14) Kim, J. W.; Aruchamy, G.; Kim, B.-K. Recent Advances in Single-Entity Electrochemistry for Metal Nanoparticle, Nanodroplet, and Bio-Entity Analysis. *TrAC Trends Anal. Chem.* **2023**, *169*, 117358. https://doi.org/10.1016/j.trac.2023.117358.

(15) Bard, A. J.; Boika, A.; Kwon, S. J.; Park, J. H.; Thorgaard, S. N. Stochastic Events in Nanoelectrochemical Systems. In *Nanoelectrochemistry*; CRC Press, 2015; pp 241–292. https://doi.org/10.1201/b18066-11.

(16) Crooks, R. M. Concluding Remarks: Single Entity Electrochemistry One Step at a Time. *Faraday Discuss.* **2016**, *193* (0), 533–547. https://doi.org/10.1039/C6FD00203J.

(17) Baker, L. A. Perspective and Prospectus on Single-Entity Electrochemistry. *J. Am. Chem. Soc.* **2018**, *140* (46), 15549–15559. https://doi.org/10.1021/jacs.8b09747.

(18) Lemay, S. G.; Kang, S.; Mathwig, K.; Singh, P. S. Single-Molecule Electrochemistry: Present Status and Outlook. *Acc. Chem. Res.* **2013**, *46* (2), 369–377. https://doi.org/10.1021/ar300169d.

(19) Bard, A. J.; Faulkner, L. R.; White, H. S. *Electrochemical Methods: Fundamentals and Applications, 3rd Edition | Wiley*, Third edition.; Wiley, 2022.

(20) Smida, H.; Thobie-Gautier, C.; Boujtita, M.; Lebègue, E. Recent Advances in Single Liposome Electrochemistry. *Curr. Opin. Electrochem.* **2022**, *36*, 101141. https://doi.org/10.1016/j.coelec.2022.101141.

(21) Smida, H.; Langlard, A.; Ameline, D.; Thobie-Gautier, C.; Boujtita, M.; Lebègue, E. Trends in Single-Impact Electrochemistry for Bacteria Analysis. *Anal. Bioanal. Chem.* **2023**, *415* (18), 3717–3725. https://doi.org/10.1007/s00216-023-04568-z.

(22) Chung, H. J.; Lee, J.; Hwang, J.; Seol, K. H.; Kim, K. M.; Song, J.; Chang, J. Stochastic Particle Approach Electrochemistry (SPAE): Estimating Size, Drift Velocity, and Electric Force of Insulating Particles. *Anal. Chem.* **2020**, *92* (18), 12226–12234. https://doi.org/10.1021/acs.analchem.0c01532.

(23) Peng, M.; Zhou, Y.-G. Impact Electrochemical Analysis of Soft Bio-Particles: A Mini Review. *Electrochem. Commun.* **2023**, *150*, 107490. https://doi.org/10.1016/j.elecom.2023.107490.

(24) Deng, Z.; Renault, C. Detection of Individual Insulating Entities by Electrochemical Blocking. *Curr. Opin. Electrochem.* **2021**, *25*, 100619. https://doi.org/10.1016/j.coelec.2020.08.001.

(25) Liu, E. Z.; Rivalta Popescu, S.; Eden, A.; Chung, J.; Roehrich, B.; Sepunaru, L. The Role of Applied Potential on Particle Sizing Precision in Single-Entity Blocking Electrochemistry. *Electrochimica Acta* **2023**, *472*, 143397. https://doi.org/10.1016/j.electacta.2023.143397.

(26) Ronspees, A. T.; Thorgaard, S. N. Blocking Electrochemical Collisions of Single E. Coli and B. Subtilis Bacteria at Ultramicroelectrodes Elucidated Using Simultaneous Fluorescence Microscopy. *Electrochimica Acta* **2018**, *278*, 412–420. https://doi.org/10.1016/j.electacta.2018.05.006.

(27) Lee, J. Y.; Kim, B.-K.; Kang, M.; Park, J. H. Label-Free Detection of Single Living Bacteria via Electrochemical Collision Event. *Sci. Rep.* **2016**, *6*, 30022. https://doi.org/10.1038/srep30022.

(28) Lebègue, E.; Costa, N. L.; Louro, R. O.; Barrière, F. Communication—Electrochemical Single Nano-Impacts of Electroactive Shewanella Oneidensis Bacteria onto Carbon Ultramicroelectrode. *J. Electrochem. Soc.* **2020**, *167* (10), 105501. https://doi.org/10.1149/1945-7111/ab9e39.

(29) Smida, H.; Langlard, A.; Thomas, L.; Thobie-Gautier, C.; Boujtita, M.; Louro, R. O.; Paquete, C. M.; Lebègue, E. Exploring the Effect of *Shewanella Oneidensis* Outer Membrane Redox Proteins in the Electrochemical Response of Single Blocking Impact Events. *Electrochimica Acta* **2024**, *488*, 144235. https://doi.org/10.1016/j.electacta.2024.144235.

(30) Deng, Z.; Elattar, R.; Maroun, F.; Renault, C. In Situ Measurement of the Size Distribution and Concentration of Insulating Particles by Electrochemical Collision on Hemispherical Ultramicroelectrodes. *Anal. Chem.* **2018**, *90* (21), 12923–12929. https://doi.org/10.1021/acs.analchem.8b03550.

(31) Bonezzi, J.; Boika, A. Deciphering the Magnitude of Current Steps in Electrochemical Blocking Collision Experiments and Its Implications. *Electrochimica Acta* **2017**, *236*, 252–259. https://doi.org/10.1016/j.electacta.2017.03.090.

(32) Ahmed, J. U.; Lutkenhaus, J. A.; Tubbs, A.; Nag, A.; Christopher, J.; Alvarez, J. C. Estimating Average Velocities of Particle Arrival Using the Time Duration of the Current Signal in Stochastic Blocking Electrochemistry. *Anal. Chem.* **2022**, *94* (48), 16560–16569. https://doi.org/10.1021/acs.analchem.2c01201.

(33) Boika, A.; Thorgaard, S. N.; Bard, A. J. Monitoring the Electrophoretic Migration and Adsorption of Single Insulating Nanoparticles at Ultramicroelectrodes. *J. Phys. Chem. B* **2013**, *117* (16), 4371–4380. https://doi.org/10.1021/jp306934g.

(34) Ho, T. L. T.; Hoang, N. T. T.; Lee, J.; Park, J. H.; Kim, B.-K. Determining Mean Corpuscular Volume and Red Blood Cell Count Using Electrochemical Collision Events. *Biosens. Bioelectron.* **2018**, *110*, 155–159. https://doi.org/10.1016/j.bios.2018.03.053.

(35) Jamali, S. S.; Wu, Y.; Homborg, A. M.; Lemay, S. G.; Gooding, J. J. Interpretation of Stochastic Electrochemical Data. *Curr. Opin. Electrochem.* **2024**, *46*, 101505. https://doi.org/10.1016/j.coelec.2024.101505.

(36) Lebègue, E.; Anderson, C. M.; Dick, J. E.; Webb, L. J.; Bard, A. J. Electrochemical Detection of Single Phospholipid Vesicle Collisions at a Pt Ultramicroelectrode. *Langmuir* **2015**, *31* (42), 11734–11739. https://doi.org/10.1021/acs.langmuir.5b03123.

(37) Shoup, D.; Szabo, A. Chronoamperometric Current at Finite Disk Electrodes. *J. Electroanal. Chem. Interfacial Electrochem.* **1982**, *140* (2), 237–245. https://doi.org/10.1016/0022-0728(82)85171-1.

(38) Sanders, J. Veusz: Scientific Plotting Package. *Astrophys. Source Code Libr.* **2023**, ascl:2307.017.

(39) RStudio Team. RStudio: Integrated Development Environment for R, 2020. http://www.rstudio.com/ (accessed 2024-04-16).

(40) Laborda, E.; Molina, A.; Batchelor-McAuley, C.; Compton, R. G. Individual Detection and Characterization of Non-Electrocatalytic, Redox-Inactive Particles in Solution by Using Electrochemistry. *ChemElectroChem* **2018**, *5* (3), 410–417. https://doi.org/10.1002/celc.201701000.

(41) Zhao, Z.; Naha, A.; Ganguli, S.; Sekretareva, A. Automated Analysis of Nano-Impact Single-Entity Electrochemistry Signals Using Unsupervised Machine Learning and Template Matching. *Adv. Intell. Syst.* **2024**, *6* (1), 2300424. https://doi.org/10.1002/aisy.202300424.

(42) Li, X.; Fu, Y.-H.; Wei, N.; Yu, R.-J.; Bhatti, H.; Zhang, L.; Yan, F.; Xia, F.; Ewing, A. G.; Long, Y.-T.; Ying, Y.-L. Emerging Data Processing Methods for Single-Entity Electrochemistry. *Angew. Chem. Int. Ed.* **2024**, *63* (17), e202316551. https://doi.org/10.1002/anie.202316551.

Table of Contents